A Review Paper on "Graphene Field Emission for Electron Microscopy"

Xiuyuan Shao [1] and Anjam Khursheed [1,2],*

[1] Department of Electrical and Computer Engineering, National University of Singapore, 4 Engineering Drive 3, Singapore 117583, Singapore

[2] Engineering Science Programme, National University of Singapore, 9 Engineering Drive 1, Singapore 117575, Singapore

* Correspondence: eleka@nus.edu.sg (A.K.); Tel.: +65-6516-2295 (A.K.)

Abstract: Although good field emission from graphene has been demonstrated from a wide variety of different micro-fabricated structures, very few of them can be used to improve the design of cold field emitters for electron microscopy applications. Most of them consist of densely packed nano-emitters, which produce a large array of defocused overlapping electron beams, and therefore cannot be subsequently defocused down to a single nano-meter electron probe. This paper reviews the kind of single-tip cathode structures suitable in cold field emission guns for instruments such as the Scanning Electron Microscopy, Transmission Electron Microscope or the Scanning Transmission Electron Microscopy, and reviews progress in fabricating them from graphene based materials.

Keywords: graphene; cold field emission; single-tip cathode; electron microscopy

1. Introduction

The Dyke group proposed a variety of applications of a cold field emission (CFE) source and formed the first company to produce CFE based commercial products in the early 1960s [1]. The successful application of CFE cathodes to electron microscopy, including both Scanning Electron Microscopy (SEM) and Scanning Transmission Electron Microscopy (STEM), was achieved by a group led by Crewe et al. in the late 1960s [2,3]. For over 40 years, state-of-the-art metal tip CFE sources used in electron microscopy suffer from many well-known practical challenges, such as an inherent Ultrahigh Vacuum (UHV) condition requirement ($<10^{-9}$ Torr) and relatively large current instabilities (~40% fall-off within the first hour), which have impeded their wide-ranging use [4]. As a result, most of the latest generation electron microscopes use the more stable and reliable Schottky electron source, which has a lower brightness (~10^8 A m^{-2} sr^{-1} V^{-1}) and higher energy spread (~0.5 eV) [5-7]. Although CFE sources have the desirable characteristics of a low energy spread (~0.3 eV) and high brightness (~10^9 A m^{-2} sr^{-1} V^{-1}), their lifetimes need to be improved (> 1 year) and their current stabilities need to be reduced (< 1%) [4,5,8].

Nanostructures in the form of nanotubes [9-12], nanotips [13], and nanowires [14,15] have the potential to be used as cathodes in CFE sources. Their large field enhancement factors stem from nanometer-scale emission sites which can, in some cases, produce electron beams with brightness values, one order of magnitude higher than the state-of-the-art single crystal tungsten cathode tips. Despite their promising electron optics performance, they have not been successfully integrated into any commercial electron microscopes, and this is largely due to the same technological difficulties faced by single crystal tungsten cathode-tips (stringent vacuum, low lifetime and high beam current fluctuations). However, in addition, they require the delicate transfer/mounting process of an individual emitter being attached to the tip of a sharpened supporting metal wire, and this is very difficult do without incurring significant misalignment or damage.

45   Since the discovery of two-dimensional (2D) graphene in 2004, graphene has attracted a lot of
46   attention as a potential candidate for CFE source emitters, due to its high aspect ratio (the lateral size
47   to the thickness) [16-18] and excellent thermal, mechanical, and electrical properties [19-22]. Excellent
48   field emission from graphene has been demonstrated from a wide variety of different micro-
49   fabricated structures, and most of them consist of densely packed nano-emitters that produce a large
50   array of defocused overlapping electron beams, and therefore cannot be subsequently defocused
51   down to a single nano-meter electron probe [23-25], making them unsuitable for electron
52   microscopy/lithography applications.
53   This paper primarily focuses on reviewing developments in the field emission of graphene based
54   emitters for electron microscopy/lithography applications. In the first part of the paper, it will
55   summarize basic field emission theory in relation to single crystal W field emitters (CFE) oriented in
56   the <310> or <111> directions and other well-developed one-dimensional (1D) nanostructure CFE
57   electron emitters. In the second part, different types of graphene field emitters will be introduced,
58   including graphene film emitters, graphene point emitters and graphene ring emitters. The main
59   theme is primarily on how graphene can be used to make single-tip cathodes in electron sources
60   suitable for electron microscopy/lithography applications, whose electron beams can be defocused
61   down to a single nano-meter electron probe. Finally, a summary and outlook are given towards the
62   future development of high brightness-high resolution CFE electron gun on graphene-based
63   nanomaterials.

64   **2. Development of a single-tip cathode CFE source**

65   *2.1. Theory of cold field electron emission*

66   Electron sources are an essential tool for investigation into a broad range of field emission
67   devices [26-30]. For electron microscopy applications, electron sources can be divided into two main
68   categories, known as thermionic and field emission [31]. A thermionic electron gun uses Joule-heating
69   induced thermal excitation to allow electrons to overcome the energy barrier between the metal tip
70   and the vacuum. The electron beam it produces is inherently incoherent, has a source size in the tens
71   of microns range, a relatively large energy spread (2 eV) and poor brightness (~10^6 A m^{-2} sr^{-1} V^{-1}). A
72   CFE electron gun overcomes these limitations by decreasing the virtual source size to about 3 nm (by
73   significantly decreasing the emission tip to about 100 nm radius) and a low energy spread to about
74   0.3 eV (operating the source at room temperature), in which electrons pass from a solid surface to the
75   vacuum by creating a high local electric field [1]. The mechanism of the electron emission process is
76   based on the Fermi-Dirac distribution for a free electron gas in the potential energy barrier between
77   the metal tip and the vacuum [32].
78   Fowler and Nordheim first found a classical theory describing the behavior of field emission
79   currents from a metallic surface in 1928 [33]. In the theory, the relationship between the emission
80   current (I) and the tip field strength (F) is expressed as,

$$I = A \frac{1.5 \times 10^{-6}}{\phi} F^2 \exp\left(-\frac{6.44 \times 10^9 \phi^{1.5}}{F}\right), \tag{1}$$

82   Where the constant A has the dimension of area [m^2], ϕ is the work function in [eV], and F is
83   the local electric field on the cathode tip, given by $F = \beta V_{\text{ext}}/d$ with β being the field enhancement
84   factor, V_{ext} the external applied voltage, and d the anode to cathode tip spacing. The cathode tip is
85   geometrically sharp, and the local electric field (F) is intensified by a factor of β on the tip surface.
86   To achieve cold field electron emission, F is typically around few volts per nanometer. A plot of
87    $\ln(I/V_{\text{ext}}^2)$ against $1/V_{\text{ext}}$ will have a slope of $m = -(6.44 \times 10^9 \phi^{1.5} d/\beta)$, the well-known FN plot.

88   *2.2. Source electron optics parameters*

89   For successful electron microscopy applications, a high source brightness (B_r) and a low energy
90   spread (ΔE) are always needed to provide a high-resolution focused electron beam. Calculation of B_r
91   requires knowledge of the virtual source size (d_v), which is given by the following expression [34]:

92
$$B_r = \frac{4I'}{\pi d_v^2 V_{\text{ext}}} \ , \qquad\qquad (2)$$

93 where I' is the angular intensity, obtained by dividing the emission current over the acceptance
94 solid angle subtending the source. Bronsgeest et al. derived an analytical formula to calculate the
95 virtual source size [34], given by the following expression:

96
$$d_v = 1.67 \frac{r_{\text{tip}}}{m_\alpha} \sqrt{\frac{<E_t>}{eV_{\text{ext}}}} \ , \qquad\qquad (3)$$

97 where r_{tip} is the tip radius and $< E_t >$ is an initial average tangential energy defined as $< E_t >$
98 $= e\hbar F/\sqrt{(8m\phi)}$, with F the local electric field strength, ϕ the work function, m_α the angular
99 magnification and $\hbar$ the reduced Planck constant. In these formulas, m_α and F can be estimated from
100 direct ray tracing simulations and when used together with an experimentally measured angular
101 intensity profile, the source brightness B_r can be estimated. For high brightness electron beam
102 applications, statistical Coulomb interactions lead to radial broadening of the virtual source size due
103 to lateral electron-electron interactions, which in turn, lower the brightness [35]. The calculation of
104 statistical Coulomb interactions within an electron source is not straightforward, since the electron
105 potential and beam size vary in the gun region. A semi-analytical technique known as the "slice
106 method" reported in the recent papers by Kruit, was introduced to do this [36]. First, the electric
107 potential distribution in the gun region is solved numerically, and then the beam size in the region is
108 determined by the simulated direct ray tracing of electron trajectories that leave the cathode-tip. The
109 gun region is subsequently divided into small segments over which the voltage and beam size is
110 assumed to remain constant, and an analytical expression is used to estimate the trajectory
111 displacement effect due to the lateral electron-electron interactions.
112   It should be noted that the method just outlined avoids the need to measure the virtual source
113 diameter d_v experimentally, this is because direct measurement of the virtual source diameter not
114 trivial. One way to achieve it is to put the source in a transmission electron microscope as the emitter
115 and obtain a magnified source image of it [7]. A different method to measure d_v is to use a
116 demagnifying lens to focus the electron beam from the gun unit into a spot which is source-size
117 dominated (relatively low contributions from lens aberrations), and then measure the spot size of the
118 beam by scanning it across a knife edge [37,38]. Another method is using a point projection
119 microscope, and this technique for measuring d_v is to place a knife edge at a small distance (a few
120 micrometers) from an emitter and to measure the angular width of the Fresnel fringes patterns
121 [12,39]. In this technique, the intensity distribution shape of the source is assumed to be a Gaussian
122 function, and the values of magnification and electron wavelength are needed to extract d_v.
123   Another important electron gun parameter, apart from brightness, is its energy spread. The
124 energy spread, through the chromatic aberration of the objective lens, degrades the final spatial
125 resolution of an electron optical system, particularly at high relative beam energy spreads (say higher
126 than 10^{-4}). Ideally, the energy distribution (ΔE) of the emitted electron beam should be as narrow as
127 possible while maintaining sufficient brightness. From the theoretical point of view, the total energy
128 distribution (TED) of electron emission in the thermal field regime was first derived by Young based
129 on the free-electron model as [40]:

130
$$P(E) = \frac{J_{FN}}{d} \left[\frac{exp\left(\frac{E-E_f}{d}\right)}{1+exp\left(\frac{E-E_f}{kT}\right)} \right] \ , \qquad\qquad (4)$$

131 where kT = 0.155 eV at room temperature, J_{FN} is the well-known Fowler-Nordheim emission
132 current density and d is the tunneling parameter given by: d = 9.76×10^{-11} $F/\phi^{1/2}$ t(y). The variable $t(y)$ is
133 a slowly-varying function of $y = 3.79×10^{-5}$ $F^{1/2}/\phi$ and can be approximated by the formula $t(y) = 1 +$
134 0.1107 $y^{1.33}$. The analytical formula is valid provided $kT/d < 0.7$ and $y < 1$. The longitudinal electron-
135 electron interactions (known as Boersch effect) will add to the intrinsic source energy spread which
136 causes an additional enlargement of the energy spread [35]. According to Knauer's model of a
137 spherical electric field around an emitter of tip radius r_{tip}, the energy broadening (in eV) due to
138 Coulomb interactions is given by [41]:

139
$$\Delta E_{\text{Boersch}} = \ 15.9 \frac{(I')^{2/3}}{r_{\text{tip}}^{1/3} V_{\text{ext}}^{1/3}} \tag{5}$$

140   *2.3. The state-of-the-art electron source used in electron microscopes*

141   The state-of-the-art electron sources used in high-resolution electron microscopy are made from
142   a single crystal W field emitter (CFE) oriented in the <310> direction with a work function of 4.5 eV
143   [4]. Figs. 1a and 1b show typical SEM images of the W<310> and W<111> CFE sources, respectively.
144   As observed in the SEM images, the emitters have a spherical apex with a radius of around 130 nm
145   at the end of the cathode-tip. For a single crystal W field emitter, the emitter axis orientation is
146   required to be <310> or <111> at the emitter apex, due to their lower work function values, and this
147   can be achieved by using a zone melting technique [42].

148
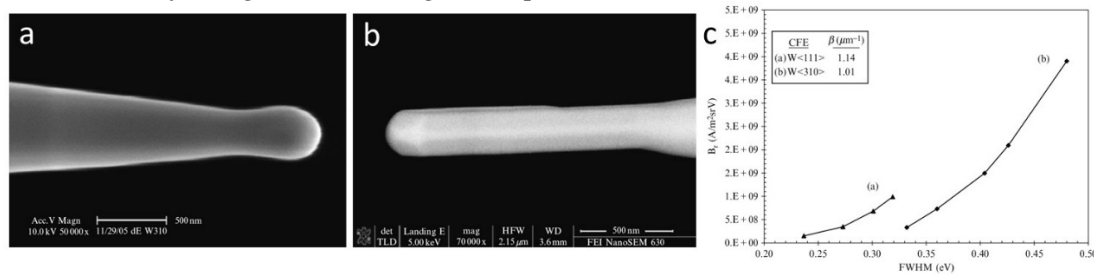
149   **Figure 1.** SEM photos of the W<310> (a) and W<111> (b) CFE sources. (c) The source reduced
150   brightness B_r versus the corresponding FWHM(E) values for the two CFE sources. Reproduced with
151   permission from [4], Copyright Elsevier, 2009.

152   The source reduced brightness (B_r) versus the FWHM(E) values for the W<310> and W<111>
153   sources are plotted in Fig 1c. For the state-of-the-art W<310> field emitter, a reduced brightness value
154   of 4×10^9 A m^{-2} sr^{-1} V^{-1} has been reported, and the measured energy spread ranges from 0.33 eV to 0.48
155   eV [4]. The relatively large values of B_r mainly come from the small values of virtual source size d_v
156   (~3 nm) and the large values of angular current density (~100 µA/sr).

157   *2.4. Nanoscale point-cathode emitters*

158   Nanostructures in the form of 1D Nanowires, Nanotubes, and Nanocones have attracted much
159   attention in past decades and have been demonstrated for many potential applications. In particular,
160   their use as potential electron field emitters exhibit excellent geometric, electrical and mechanical
161   properties, as compared to conventional metallic cold field emitters [43-46]. However, there are also
162   significant technical challenges that have yet to be resolved.
163   Generally, preparation of an individual nanoscopic CFE electron emitter is an extremely labor-
164   intensive delicate process. To mount a single nanowire or nanotube onto a supporting tip, the most
165   common method is to use microscopic manipulators under the observation of an electron microscope.
166   Fig. 2a and 2c show a single LaB$_6$ nanowire [15] and a single CNT nanotube [9] mounted on a
167   sharpened W tip, respectively. The ends of the emitter were deposited with platinum (or carbon) by
168   electron beam induced deposition (EBID) in order to make good thermal contact and the final emitter
169   structure is fitted into an electron gun unit is shown in Fig. 2b, and its inset. Figs. 2d and 2e show the
170   mounting procedure for a carbon cone nanotip (CCnT) [13], where a CCnT was welded onto the apex
171   of the supporting tip by using a gas injecting system. The whole process has a very high probability
172   of incurring misalignment and damage
173   These nanoscale point-cathode emitters also have the limitation that they need to be operated in
174   an UHV level, in the 10^{-11} to 10^{-10} Torr range. For a LaB$_6$ point-cathode emitter with a dimeter of nearly
175   60 nm, a maximum reduced brightness (B_r) of 2.77×10^{11} A m^{-2} sr^{-1} V^{-1} and energy spread value of 0.367
176   eV have been reported in a vacuum with a base pressure of 10^{-10} Torr. The short-term stability profile
177   of the LaB$_6$ point-cathode is 0.32% over 60 seconds, and the emission current deviates from the mean
178   within 5% throughout a week-long test. For the CNT and CCnT point-cathode emitters with
179   diameters of around 10 nm, the source electron optics parameters were reported to be 8.2×10^9 A m^{-2}

180 sr^{-1} V^{-1}, 0.48 eV, and 1.6×10^9 A m^{-2} sr^{-1} V^{-1}, 0.32 eV respectively. The vacuum pressure requirements
181 are even more stringent for CNTs and CCnT point-cathode emitters, typically around 10^{-11} Torr. It
182 was found there exists some unrecoverable structure damage to the CNT during electron emission
183 under the high vacuum conditions of 9×10^{-8} Torr, and this leads to emission reduction or failure [47].
184 In addition to its inherent UHV requirements, the CNT emitter is reported to have relatively large
185 fluctuations in emission current, e.g. up to 24% for an emission current of about 2 μA over 6 hours
186 with a sampling rate of 3×10^{-3} Hz.

187
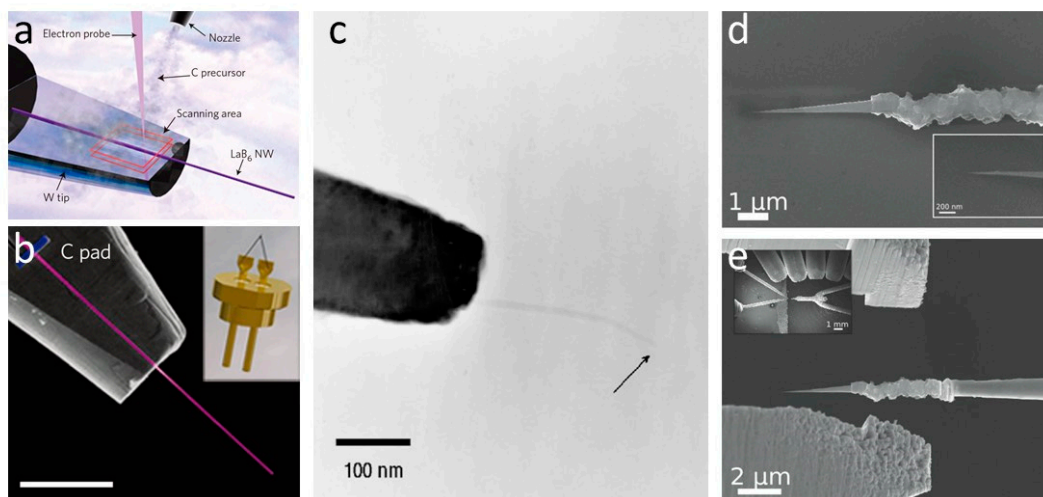
188 **Figure 2.** Well-developed nanowire, nanotube, and nanocone point-cathode cold field emitters. (a)
189 Illustration showing the electron beam deposition process to fix a LaB$_6$ NW onto a W needle. (b) SEM
190 image showing the finished LaB$_6$ NW emitter and the complete emitter assembly used for field-
191 emission SEM, scale bar, 10 μm. Reproduced with permission from [15], Copyright Springer Nature,
192 2015; (c) TEM image of a very thin and short nanotube sample. Reproduced with permission from [9],
193 Copyright Elsevier, 2003; (d) View of part of the starting CCnT object. (e) Resulting new tip after
194 welding the carbon microfiber to the tungsten tip. The inset displays the whole set-up inside the dual
195 beam. Reproduced with permission from [13], Copyright Elsevier, 2012.

196 These nanoscale CFE electron sources have not as yet been successfully integrated in any
197 commercial electron microscopes due to the aforementioned significant technical challenges, and
198 studies of nanowire, nanotube, and nanocone based cold field emitters have remained at the research
199 level. Meanwhile, other developments in CFE electron emitter research have come from the use of
200 materials such as graphene.

3. Graphene based cold field emitters

202 Fast development of 2D graphene in recent years has led to a variety of different applications
203 for field emission based devices [19]. Compared with other metallic or 1D nanoscale CFE electron
204 sources, graphene is well known for possessing several desirable properties: (1) it has excellent
205 thermal, mechanical, and electrical characteristics [16,20], (2) its work function can be significantly
206 lowered both by direct contact with metals (effectively doping it), and through the application of
207 intense electric fields [48,49], (3) it is extremely flexible. Graphene CFE electron sources fall into two
208 main categories: the single-tip cathode field nano-emitter (which includes point cathodes and ring
209 cathodes) and graphene film cathodes, which consist of densely packed graphene nano-emitters.
210 Only the former can be used for electron microscopy applications, as the latter produces a large array
211 of defocused overlapping electron virtual sources that cannot be subsequently defocused down to a
212 single nano-sized probe.

213
214
215

3.1. Graphene film emitters

To achieve successful electron emission from graphene, it is crucial to orientate thin graphene edges or control the dimension of graphene protrusions on some supporting substrate, in order to sufficiently enhance the applied electric field to produce quantum tunneling. Until now, many emerging technologies have become available for fabricating vertically aligned graphene nanosheets (VG) or graphene protrusions. The plasma-enhanced chemical vapor deposition (PECVD) is the most widely used way to synthesize large-scale VG graphene films [50], which offers the advantages of a lower substrate temperature and higher growth selectivity (Fig. 3a). Koh et al. presented a pulsed laser deposition (PLD) method [51] to directly fabricate graphene thin film onto metal nano-sized Spindt tips by using the transformation of solid carbon deposited from a pulsed laser system at low temperature (Fig. 3b). The main drawback of these two deposition methods remains the difficulty of controlling the graphene film ordering and density with problems arising due to the screening effect [52,53].
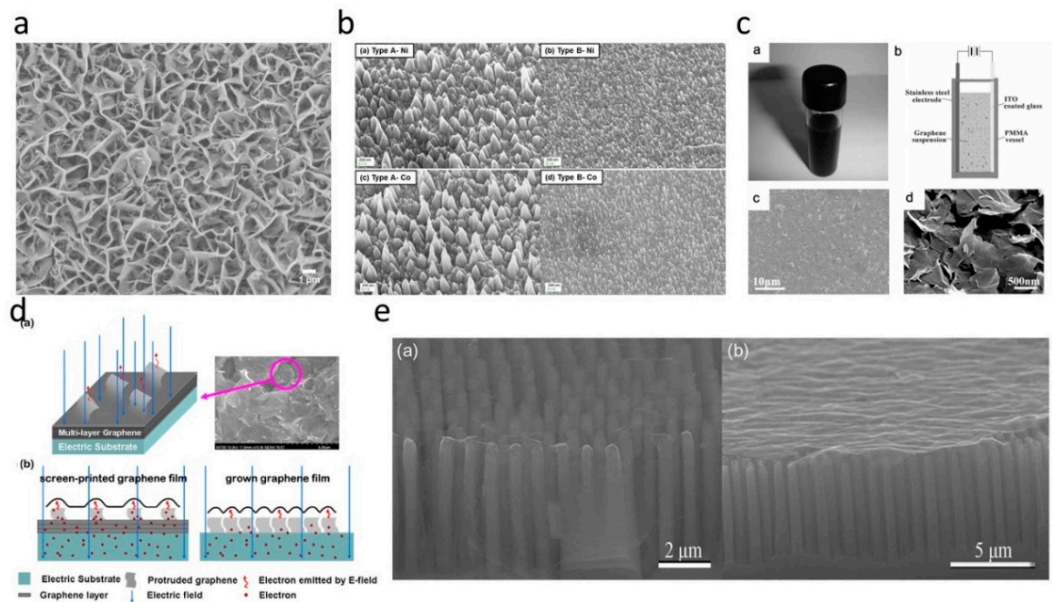
Figure 3. SEM images of microfabricated graphene film emitters. (a) Top view SEM micrograph of as grown FLG by microwave PECVD. Reproduced with permission from [50], Copyright AIP, 2008; (b) Graphene onto metal nano-Spindt tip by pulsed laser deposition. Reproduced with permission from [51], Copyright Wiley, 2014; (c) Graphene films prepared by electrophoretic deposition. Reproduced with permission from [54], Copyright Wiley, 2009; (d) Screen-printed graphene films. Reproduced with permission from [55], Copyright IOP, 2009; (e) Hybrid structures of graphene stretched on patterned and size-controllable Si nanowires. Reproduced with permission from [24], Copyright Springer Nature, 2015.

Wu et al. applied the electrophoretic deposition (EPD) technique [54] to fabricate large area homogeneous single-layer graphene films, and this processing technique is more economic and versatile compared to PECVD (Fig. 3b). Screen printing technology is a sophisticated technology widely used in large-scale applications coating on various substrates. A screen-printed graphene cathode was fabricated by Qian et al. [55] using high-yield graphene prepared by a modified Hummers method and a hydrazine hydrate reduction process (Fig. 3d). Another efficient way to produce uniform nanometer-scale graphene protrusions is through transferring graphene onto some sharp supporting substrates (Fig. 3e) [23,24,56]. However, the exfoliated graphene by using either screen printing technologies, or electrophoretic deposition, or simple transfer have been found to lead to many defects to the as-grown graphene, that degrades its physical properties [57-59]. For graphene film emitters, high current densities, around 23 mA cm^{-2}, have been reported with good stability over a period of several hours [54]. Current density here, is calculated by dividing the total measured emission current by the average area on the substrate occupied by emitter sites. Although

251   not suitable for electron microscopy applications, graphene film emitters are very useful for many
252   non-focused electron beam applications, like flat panel display [27,60], X-ray sources [61-63], etc.

253   *3.2. Graphene point-cathode field emitters*

254   Until now, graphene point-cathode field emitters for electron microscopy applications have been
255   rarely studied due to the difficulties inherent in controlling graphene morphology. Tsai et al. [64]
256   reported an idea of overlaying an ultra-thin (~1 nm) graphene flake on to a blunted tungsten probe
257   by van der Waals forces, as shown in Fig. 4a, which would make it applicable to single-column
258   electron beam microscopy applications. However, this loosely hanging ultra-thin freestanding
259   graphene flake is not suitable for practical applications, since the graphene can easily be damaged or
260   detached from its supporting probe. More importantly, the emitting surface is not circular, it spans a
261   few micrometers along one direction, and this means it can't be subsequently defocused down to a
262   single nano-meter electron spot.

263
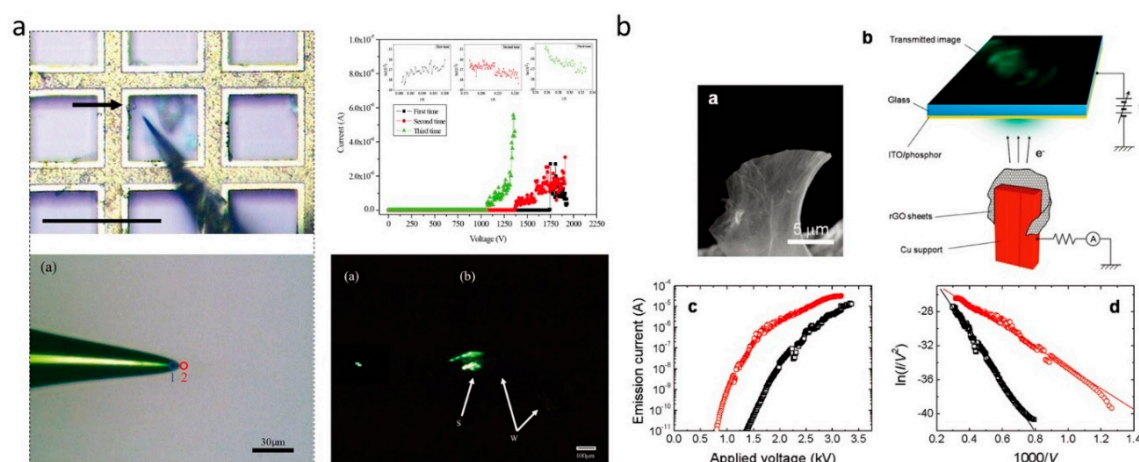
264   **Figure 4.** Images of graphene edge field emitters and field emission characteristics. (a) Field emission
265   from individual freestanding graphene edge. Reproduced with permission from [64], Copyright
266   Wiley, 2013; (b) Field emission from atomically thin edges of reduced graphene oxide. Reproduced
267   with permission from [69], Copyright ACS publications, 2011.

268   For most single point field emitters, the emission current is surface sensitive and the adsorption
269   of any gas molecules will increase the surface work function [14,65]. A high emission current under
270   excessive applied voltage ionizes many gas molecules around the emission surface and eventually
271   triggers a vacuum arc. Therefore, the practical use of cold field emitters in electron microscopes
272   typically requires cathode flashing at regular intervals to remove the residual contaminant molecules.
273   Endo et al. [66] reported that CFE electron sources can be cleaned by in situ Joule heating during the
274   emission process in high vacuum (HV) conditions, which is well known as a "conditioning" process
275   in many cold field emission experiments [67-69]. For example, during the first and second cycle of
276   voltage ramping up from the graphene flake overlaid on the tungsten probe (Fig. 4a), the current-
277   applied voltage characteristic presents a typical conditioning process, which is observed to deviate
278   from the conventional FN plot. The third cycle of electron emission shows a well fitted FN plot with
279   an emission current up to 6 μA. Similar work has been done by other researchers studying the field
280   emission characteristics from reduced graphene oxide (Fig. 4b) and carbon nanowalls, and they have
281   obtained high emission current, around several tens of micro-amps [69,70]. However, none of these
282   kinds of emission conditioning experiments on CFE graphene flakes have direct application for
283   electron microscopy, where a single point graphene source is required.

284   Recently, the research group at the National University of Singapore, led by A. Khursheed, have
285   presented the development of a completely new type of cold field emission electron source (Fig. 5a),
286   a Graphene-Ni point cathode for electron microscopy systems [71]. They present a way of
287   overcoming the morphological problems associated with micro-fabricating single-tip graphene
288   emitters, by coating it on to a sharpened wire metal wire tip. In doing so, they have overcome many

289   of the practical difficulties associated with conventional metallic tungsten CFE sources, such as
290   misalignment, damage, stringent vacuum requirements, and current instabilities. They reported
291   stable field emission results from a graphene coated nickel wire tip in HV conditions (4×10^{-8} Torr),
292   where the tip diameter is in the submicron to micron range, over a factor of three times larger than
293   conventional single crystal tungsten tip sizes, sizes that are comparable to the Schottky field emitter
294   tip.

295
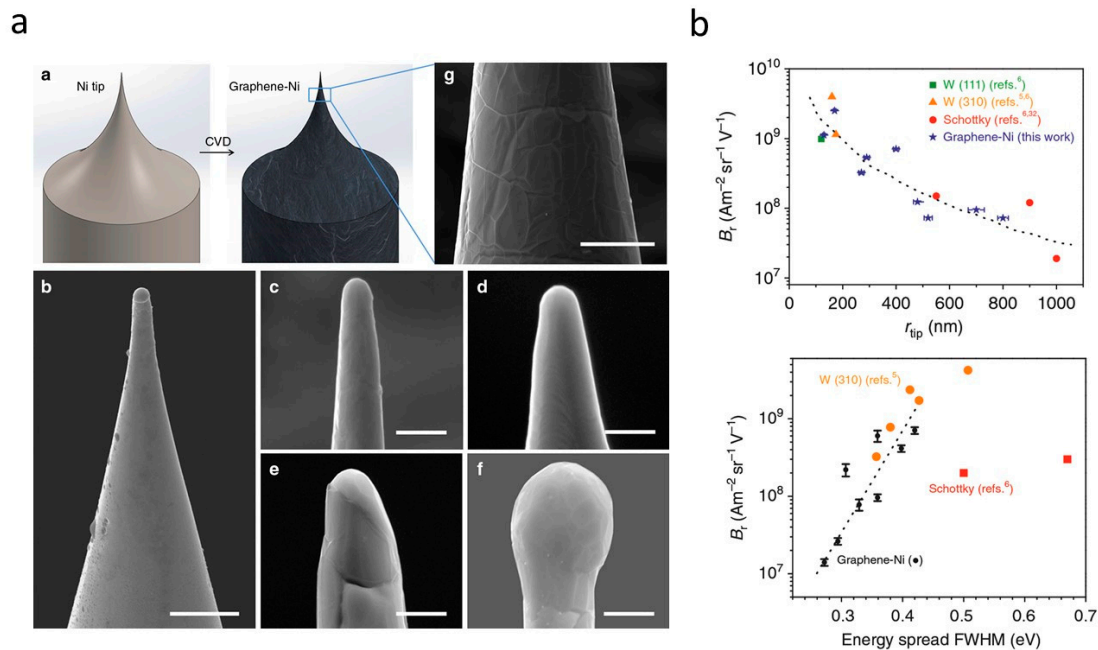
Figure 5. Graphene coated point cathode field emitter. (a) SEM images of graphene coated point
cathode emitter. Reproduced with permission from [71], Copyright Springer Nature, 2018; (b) Source
brightness and energy spread. Reproduced with permission from [71], Copyright Springer Nature,
2018.

300   The Graphene-Ni point cathode was fabricated by a two-step process, which consists firstly of
301   an electrochemical etching process to obtain a sharp Ni tip, and secondly, a graphene coating step of
302   chemical vapor deposition (CVD). The Graphene-Ni point cathode was shown to have a maximum
303   emission current of about 5 µA, and the experimental results do not indicate any obvious need for
304   regular flashing (heating) of the cathode. More importantly, experimental results demonstrate that
305   the large diameter Graphene-Ni point cathodes are capable of emitting over a few micro-amps of
306   current stably for over 72 hours, and no emitter failure was observed. In their study, direct ray tracing
307   simulations of electron trajectory paths leaving the emitter surface were carried out to estimate m_α
308   and F, from which the virtual source size d_v and gun brightness B_r were then calculated by using Eqs.
309   2 and 3. The source brightness values range from 7×10^7 A m^{-2} sr^{-1} V^{-1} to 2.51×10^9 A m^{-2} sr^{-1} V^{-1} for a
310   cathode tip radii range of 130 nm to 800 nm. There is a trade-off between the source brightness value
311   and the tip size. On the one hand, a larger tip size has a greater emission area, thereby having a better
312   current stability and can operate in much less stringent vacuum conditions, predicted by the root
313   mean square (RMS) noise ratio varying inversely with the emission area [72]. One the other hand, a
314   larger tip size has a larger virtual source size and lower source brightness value. This trade-off is
315   applicable to all CFE sources, and most of the previous studies on CNT, LaB$_6$, and CCnT tips sought
316   to maximized gun brightness at the expense of gun current stability and stringent vacuum
317   requirements. Another stand out feature of the Graphene-Ni point cathodes is their low energy
318   spread (Fig. 5b). The lowest reported energy spread is 0.246 eV obtained from a tip with a radius of
319   500 nm, and these properties make cold field emission sources the best type of electron source for
320   forming nano-size electron probes combined with high current intensity. Therefore, the promising
321   prospect of using Graphene-based CFE cathodes for high brightness high resolution electron
322   microscopy applications has recently been established.

323   *3.3. Graphene ring-cathode field emitters*

324   Khursheed first proposed the idea of using a ring-cathode emitter for combining high spatial
325   resolution with high beam current for focused electron beam applications in 2013 [73,74]. Khursheed
326   presented electron focused beam designs based upon using ring-cathodes together with off-axis
327   aberration correction techniques. The first step towards a practical implementation of this idea is to
328   develop a ring-cathode emitter. The proposal of a field emission ring-cathode gun unit has the
329   advantage of intrinsically being a large area field emitter, and it is therefore expected to overcome
330   the well-known disadvantage of conventional point-cathode field emitters having relatively low total
331   current (compared to earlier larger cathode electron gun designs). The much larger emission area of
332   a ring-cathode field emitter, compared to a point-cathode field emitter is also expected to provide it
333   with greater current stability.

334   Nguyen et al. [75] reported a versatile and robust method based on graphene growth on Ni
335   templates and thermo-assisted removal of poly(methyl methacrylate) (PMMA) for fabrication of
336   macroscopic and freestanding tubular graphene (TG) architectures. The TG architectures have a
337   diameter of 50 μm with a wall thickness in the range of 2.1-2.9 nm. The individual TG emitter can
338   produce an extremely high emission current, up to 0.46 mA at a very low external applied electric
339   field of 0.68 V μm^{-1}. This most likely comes from ultrathin edges on graphitic walls, which consist of
340   a great number of field emission sites. Another important observation is that the TG CFE electron
341   source has good current stability and the stability is maintainable for days under HV conditions
342   (2.2×10^{-8} Torr). However, one limitation of TG architectures fabricated by Nguyen et al. is that the
343   edges are very jagged rather than being smooth, making it hard to be directly used as a CFE electron
344   source for electron microscopy applications. Moreover, transfer and alignment of such a large
345   diameter graphene tube is an extremely delicate process.

346
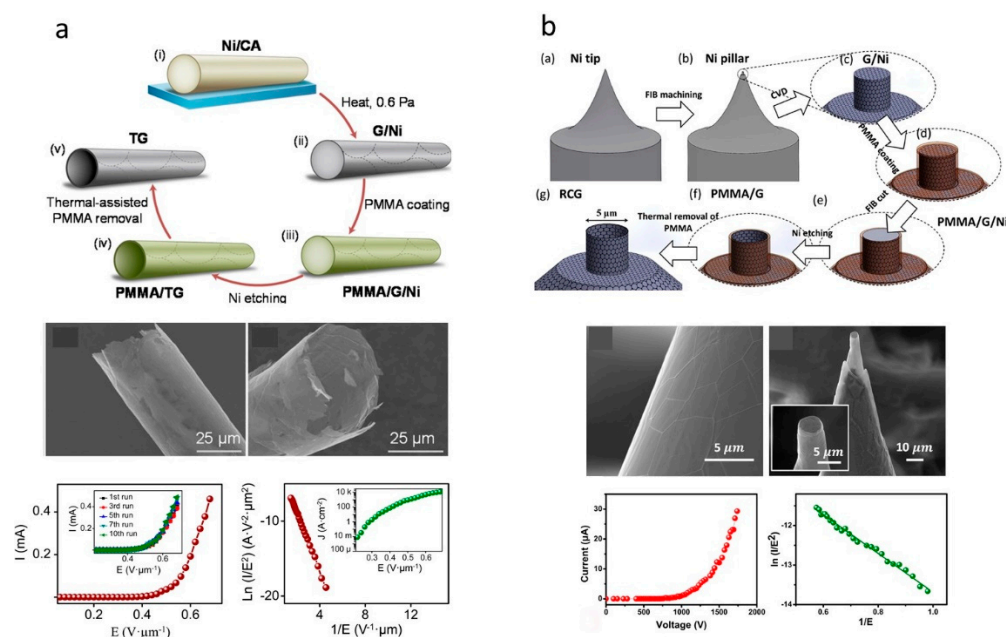
347   **Figure 6.** Graphene ring-cathode field emitter. (a) Macroscopic, freestanding, and tubular graphene
348   architectures. Reproduced with permission from [75], Copyright ACS publications, 2015; (b) A few-
349   layer graphene ring-cathode field emitter. Reproduced with permission from [76], Copyright Elsevier,
350   2016;

351   Shao et al. [76] reported an in-situ fabrication technique, eliminating any transfer and alignment
352   process. They obtained a graphene ring emitter, which consists of a graphene tube grown in-situ on
353   a sharp nickel wire tip. The diameter of the tubular graphene is about 5 μm while the edge of the tube
354   is approximately 2.7 nm. They have obtained high emission current of ~30 μA at the relatively low
355   applied field of ~1.75 V/mm. The ring-cathode field emitter is a new type of field emitter source, and
356   suitable electron ring-focused beam columns will first need to be designed for it. When that is

357 achieved, it is expected to a wide variety of applications in subjects such as lithography, mass
358 spectrometer, X-ray tube and accelerator physics.

359 **4. Conclusions**

360 High brightness, low energy spread and good current stability are critical for CFE electron
361 sources for electron microscopy applications. Although considerable research has been carried out
362 into developing single crystal tungsten and other 1D nanostructure-based field emitters, they have
363 as yet, faced many practical technological difficulties, such as stringent UHV requirements, poor
364 current stability and fast emission decay. Therefore, other ways to make CFE electron sources need
365 to be investigated. With the fast development of 2D graphene in recent years, graphene has been
366 proven to have ultra-high aspect ratios, good electric conductivity, chemical inertness and mechanical
367 hardness, and these properties make graphene based field emitters an attractive possible alternative.
368 Three types of graphene-based field emitters have been highlighted in this review: graphene film
369 emitters, graphene point/edge-cathode emitters, and graphene ring-cathode emitters. Most graphene
370 field emitters proposed and studied so however, involve field emission from multiple emission sites,
371 and are therefore not suitable for electron microscopy applications.

372 This paper has highlighted some recent promising developments in the category of single-point
373 and ring-shaped graphene field emitters for electron microscopy applications, however, the
374 investigation of graphene field emitters is still in an early stage of development, and there is still
375 much room for further improvement. More emission characterization tests need to be performed,
376 ones that can measure the source virtual source size, transverse coherent length, emission under a
377 variety of different vacuum conditions, and emitter lifetime need to be made. An electron gun unit
378 that can accommodate promising graphene emitters, which has its optical axis well aligned to the
379 central axis of the cathode still needs to be developed. Beyond that, electron guns based upon the
380 new class of graphene based field emitters need to be fitted on to electron microscopes, and their
381 performance critically compared to convention systems, in terms of parameters such as image
382 resolution and signal-to-noise.

383 **Acknowledgments:** This work is funded by the National Research Foundation (NRF) Competitive Research
384 Programme (CRP) award # NRFCRP13-2014-04 titled "Micro-fabricated Ring Carbon Nanotube electron/ion
385 sources".

386 **Conflicts of Interest:** The authors declare no conflict of interest.

387 **References**

388 1. Dyke, W.; Dolan, W. Field emission. Adv. Electron. Electron Phys. 1956, 8, 89-185.
389 2. Crewe, A.; Wall, J.; Welter, L. A high-resolution scanning transmission electron microscope. J. Appl. Phys.
390   1968, 39, 5861-5868.
391 3. Crewe, A.V.; Isaacson, M.; Johnson, D. A simple scanning electron microscope. Rev. Sci. Instrum. 1969, 40,
392   241-246.
393 4. Swanson, L.; Schwind, G. A review of the cold-field electron cathode. Adv. Imaging Electron Phys. 2009,
394   159, 63-100.
395 5. Schwind, G.; Magera, G.; Swanson, L. Comparison of parameters for schottky and cold field emission
396   sources. J. Vac. Sci. Technol. B 2006, 24, 2897-2901.
397 6. Tuggle, D.; Swanson, L. Emission characteristics of the zro/w thermal field electron source. J. Vac. Sci.
398   Technol. B 1985, 3, 220-223.
399 7. Fransen, M.; Overwijk, M.; Kruit, P. Brightness measurements of a zro/w schottky electron emitter in a
400   transmission electron microscope. Appl. Surf. Sci. 1999, 146, 357-362.
401 8. Crewe, A.; Eggenberger, D.; Wall, J.; Welter, L. Electron gun using a field emission source. Rev. Sci. Instrum.
402   1968, 39, 576-583.
403 9. De Jonge, N.; Van Druten, N. Field emission from individual multiwalled carbon nanotubes prepared in
404   an electron microscope. Ultramicroscopy 2003, 95, 85-91.
405 10. Bonard, J.-M.; Dean, K.A.; Coll, B.F.; Klinke, C. Field emission of individual carbon nanotubes in the
406   scanning electron microscope. Phys. Rev. Lett. 2002, 89, 197602.

407   11.   Fransen, M.; Van Rooy, T.L.; Kruit, P. Field emission energy distributions from individual multiwalled
408   carbon nanotubes. Appl. Surf. Sci. 1999, 146, 312-327.
409   12.   De Jonge, N.; Lamy, Y.; Schoots, K.; Oosterkamp, T.H. High brightness electron beam from a multi-walled
410   carbon nanotube. Nature 2002, 420, 393.
411   13.   Houdellier, F.; De Knoop, L.; Gatel, C.; Masseboeuf, A.; Mamishin, S.; Taniguchi, Y.; Delmas, M.;
412   Monthioux, M.; Hÿtch, M.; Snoeck, E. Development of tem and sem high brightness electron guns using
413   cold-field emission from a carbon nanotip. Ultramicroscopy 2015, 151, 107-115.
414   14.   Yeong, K.; Thong, J. Field-emission properties of ultrathin 5 nm tungsten nanowire. J. Appl. Phys. 2006,
415   100, 114325.
416   15.   Zhang, H.; Tang, J.; Yuan, J.; Yamauchi, Y.; Suzuki, T.T.; Shinya, N.; Nakajima, K.; Qin, L.-C. An ultrabright
417   and monochromatic electron point source made of a lab 6 nanowire. Nat. Nanotechnol. 2016, 11, 273.
418   16.   Novoselov, K.S.; Geim, A.K.; Morozov, S.; Jiang, D.; Katsnelson, M.; Grigorieva, I.; Dubonos, S.; Firsov; AA.
419   Two-dimensional gas of massless dirac fermions in graphene. Nature 2005, 438, 197.
420   17.   Xiao, Z.; She, J.; Deng, S.; Tang, Z.; Li, Z.; Lu, J.; Xu, N. Field electron emission characteristics and physical
421   mechanism of individual single-layer graphene. Acs Nano 2010, 4, 6332-6336.
422   18.   Lei, W.; Li, C.; Cole, M.T.; Qu, K.; Ding, S.; Zhang, Y.; Warner, J.H.; Zhang, X.; Wang, B.; Milne, W.I. A
423   graphene-based large area surface-conduction electron emission display. Carbon 2013, 56, 255-263.
424   19.   Geim, A.K.; Novoselov, K.S. The rise of graphene. Nat. Mater. 2007, 6, 183.
425   20.   Balandin, A.A.; Ghosh, S.; Bao, W.; Calizo, I.; Teweldebrhan, D.; Miao, F.; Lau, C.N. Superior thermal
426   conductivity of single-layer graphene. Nano Lett. 2008, 8, 902-907.
427   21.   Neto, A.C.; Guinea, F.; Peres, N.M.; Novoselov, K.S.; Geim, A.K. The electronic properties of graphene.
428   Rev. Mod. Phys. 2009, 81, 109.
429   22.   Lee, C.; Wei, X.; Kysar, J.W.; Hone, J. Measurement of the elastic properties and intrinsic strength of
430   monolayer graphene. science 2008, 321, 385-388.
431   23.   Ye, D.; Moussa, S.; Ferguson, J.D.; Baski, A.A.; El-Shall, M.S. Highly efficient electron field emission from
432   graphene oxide sheets supported by nickel nanotip arrays. Nano Lett. 2012, 12, 1265-1268.
433   24.   Lv, S.; Li, Z.; Liao, J.; Wang, G.; Li, M.; Miao, W. Optimizing field emission properties of the hybrid
434   structures of graphene stretched on patterned and size-controllable sinws. Sci. Rep. 2015, 5, 15035.
435   25.   Zhang, Y.; Du, J.; Tang, S.; Liu, P.; Deng, S.; Chen, J.; Xu, N. Optimize the field emission character of a
436   vertical few-layer graphene sheet by manipulating the morphology. Nanotechnology 2011, 23, 015202.
437   26.   Hernandez-Garcia, C.; O Shea, P.G.; Stutzman, M.L. Electron sources for accelerators. Phys. today 2008, 61,
438   44.
439   27.   Choi, W.; Chung, D.; Kang, J.; Kim, H.; Jin, Y.; Han, I.; Lee, Y.; Jung, J.; Lee, N.; Park, G. Fully sealed, high-
440   brightness carbon-nanotube field-emission display. Appl. Phys. Lett. 1999, 75, 3129-3131.
441   28.   Saito, Y.; Uemura, S. Field emission from carbon nanotubes and its application to electron sources. Carbon
442   2000, 38, 169-182.
443   29.   Barber, M.; Bordoli, R.; Sedgwick, R.; Tyler, A. Fast atom bombardment of solids as an ion source in mass
444   spectrometry. Nature 1981, 293, 270.
445   30.   Khursheed, A. Scanning electron microscope. Google Patents: 2007.
446   31.   Khursheed, A. Scanning electron microscope optics and spectrometers. World scientific: 2011.
447   32.   Murphy, E.L.; Good Jr, R. Thermionic emission, field emission, and the transition region. Phys. Rev. 1956,
448   102, 1464.
449   33.   Fowler, R.H.; Nordheim, L. Electron emission in intense electric fields. Proc. R. Soc. Lond. A 1928, 119, 173-
450   181.
451   34.   Bronsgeest, M.; Barth, J.; Swanson, L.; Kruit, P. Probe current, probe size, and the practical brightness for
452   probe forming systems. J. Vac. Sci. Technol. B 2008, 26, 949-955.
453   35.   Kruit, P.; Jansen, G.H. Space charge and statistical coulomb effects. Handbook of Charged Particle Optics
454   1997, 2.
455   36.   Cook, B.; Verduin, T.; Hagen, C.; Kruit, P. Brightness limitations of cold field emitters caused by coulomb
456   interactions. J. Vac. Sci. Technol. B 2010, 28, C6C74-C76C79.
457   37.   Kratschmer, E.; Rishton, S.; Kern, D.; Chang, T. Quantitative analysis of resolution and stability in
458   nanometer electron beam lithography. J. Vac. Sci. Technol. B 1988, 6, 2074-2079.
459   38.   Rishton, S.; Beaumont, S.; Wilkinson, C. Measurement of the profile of finely focused electron beams in a
460   scanning electron microscope. J. Phys. E: Sci. Instrum. 1984, 17, 296.

461   39.   Fransen, M.; Damen, E.; Schiller, C.; van Rooy, T.; Groen, H.; Kruit, P. Characterization of ultrasharp field
462   emitters by projection microscopy. Appl. Surf. Sci. 1996, 94, 107-112.
463   40.   Young, R.D. Theoretical total-energy distribution of field-emitted electrons. Phys. Rev. 1959, 113, 110.
464   41.   Knauer, W. Energy broadening in field emitted electron and ion-beams. Optik 1981, 59, 335-354.
465   42.   Dyke, W.; Charbonnier, F.; Strayer, R.; Floyd, R.; Barbour, J.; Trolan, J. Electrical stability and life of the
466   heated field emission cathode. J. Appl. Phys. 1960, 31, 790-805.
467   43.   Ajayan, P. Nanotubes from carbon. Chem. Rev. 1999, 99, 1787-1800.
468   44.   Berber, S.; Kwon, Y.-K.; Tománek, D. Unusually high thermal conductivity of carbon nanotubes. Phys. Rev.
469   Lett. 2000, 84, 4613.
470   45.   Ebbesen, T.; Lezec, H.; Hiura, H.; Bennett, J.; Ghaemi, H.; Thio, T. Electrical conductivity of individual
471   carbon nanotubes. Nature 1996, 382, 54.
472   46.   Zhang, H.; Tang, J.; Zhang, Q.; Zhao, G.; Yang, G.; Zhang, J.; Zhou, O.; Qin, L.C. Field emission of electrons
473   from single lab6 nanowires. Adv. Mater. 2006, 18, 87-91.
474   47.   Jin, C.; Wang, J.; Wang, M.; Su, J.; Peng, L.-M. In-situ studies of electron field emission of single carbon
475   nanotubes inside the tem. Carbon 2005, 43, 1026-1031.
476   48.   Giovannetti, G.; Khomyakov, P.; Brocks, G.; Karpan, V.v.; Van den Brink, J.; Kelly, P.J. Doping graphene
477   with metal contacts. Phys. Rev. Lett. 2008, 101, 026803.
478   49.   Kwon, K.C.; Choi, K.S.; Kim, B.J.; Lee, J.-L.; Kim, S.Y. Work-function decrease of graphene sheet using alkali
479   metal carbonates. J. Phys. Chem. C 2012, 116, 26586-26591.
480   50.   Malesevic, A.; Kemps, R.; Vanhulsel, A.; Chowdhury, M.P.; Volodin, A.; Van Haesendonck, C. Field
481   emission from vertically aligned few-layer graphene. J. Appl. Phys. 2008, 104, 084301.
482   51.   Koh, A.T.; Foong, Y.M.; Yusop, Z.; Tanemura, M.; Chua, D.H. Low temperature direct of graphene onto
483   metal nano-spindt tip with applications in electron emission. Adv. Mater. Interfaces 2014, 1.
484   52.   Suh, J.S.; Jeong, K.S.; Lee, J.S.; Han, I. Study of the field-screening effect of highly ordered carbon nanotube
485   arrays. Appl. Phys. Lett. 2002, 80, 2392-2394.
486   53.   Bonard, J.M.; Weiss, N.; Kind, H.; Stöckli, T.; Forró, L.s.; Kern, K.; Chatelain, A. Tuning the field emission
487   properties of patterned carbon nanotube films. Adv. Mater. 2001, 13, 184-188.
488   54.   Wu, Z.S.; Pei, S.; Ren, W.; Tang, D.; Gao, L.; Liu, B.; Li, F.; Liu, C.; Cheng, H.M. Field emission of single-
489   layer graphene films prepared by electrophoretic deposition. Adv. Mater. 2009, 21, 1756-1760.
490   55.   Qian, M.; Feng, T.; Ding, H.; Lin, L.; Li, H.; Chen, Y.; Sun, Z. Electron field emission from screen-printed
491   graphene films. Nanotechnology 2009, 20, 425702.
492   56.   Hwang, J.O.; Lee, D.H.; Kim, J.Y.; Han, T.H.; Kim, B.H.; Park, M.; No, K.; Kim, S.O. Vertical zno
493   nanowires/graphene hybrids for transparent and flexible field emission. J. Mater. Chem. 2011, 21, 3432-
494   3437.
495   57.   Hallam, T.; Berner, N.C.; Yim, C.; Duesberg, G.S. Strain, bubbles, dirt, and folds: A study of graphene
496   polymer-assisted transfer. Adv. Mater. Interfaces 2014, 1.
497   58.   Li, X.; Zhu, Y.; Cai, W.; Borysiak, M.; Han, B.; Chen, D.; Piner, R.D.; Colombo, L.; Ruoff, R.S. Transfer of
498   large-area graphene films for high-performance transparent conductive electrodes. Nano Lett. 2009, 9,
499   4359-4363.
500   59.   Suk, J.W.; Kitt, A.; Magnuson, C.W.; Hao, Y.; Ahmed, S.; An, J.; Swan, A.K.; Goldberg, B.B.; Ruoff, R.S.
501   Transfer of cvd-grown monolayer graphene onto arbitrary substrates. ACS nano 2011, 5, 6916-6924.
502   60.   Yang, C.; Liu, N.; Zeng, W.; Long, F.; Song, Z.; Su, J.; Li, L.; Zou, Z.; Fang, G.; Xiong, L. Superelastic and
503   ultralight electron source from modifying 3d reduced graphene aerogel microstructure. Nano Energy 2017,
504   33, 280-287.
505   61.   Lee, H.R.; Lee, S.W.; Shikili, C.; Kang, J.S.; Lee, J.; Park, K.C. Enhanced electron emission of paste cnt
506   emitters with nickel buffer layer and its x-ray application. J. Nanosci. Nanotechnol. 2016, 16, 12053-12058.
507   62.   Sugie, H.; Tanemura, M.; Filip, V.; Iwata, K.; Takahashi, K.; Okuyama, F. Carbon nanotubes as electron
508   source in an x-ray tube. Appl. Phys. Lett. 2001, 78, 2578-2580.
509   63.   Lee, Y.Z.; Burk, L.; Wang, K.-h.; Cao, G.; Lu, J.; Zhou, O. Carbon nanotube based x-ray sources: Applications
510   in pre-clinical and medical imaging. Nucl. Instrum. Meth. A 2011, 648, S281-S283.
511   64.   Tsai, J.T.; Chu, T.Y.; Shiu, J.Y.; Yang, C.S. Field emission from an individual freestanding graphene edge.
512   Small 2012, 8, 3739-3745.
513   65.   Kleint, C. Electron emission noise. Surf. Sci. 1988, 200, 472-489.

66. Endo, Y.; Honjo, I.; Goto, S. Microelectron gun with silicon field emitter. J. Vac. Sci. Technol. B 1998, 16, 3082-3085.

67. Purcell, S.; Vincent, P.; Journet, C.; Binh, V.T. Hot nanotubes: Stable heating of individual multiwall carbon nanotubes to 2000 k induced by the field-emission current. Phys. Rev. Lett. 2002, 88, 105502.

68. Semet, V.; Binh, V.T.; Vincent, P.; Guillot, D.; Teo, K.; Chhowalla, M.; Amaratunga, G.; Milne, W.; Legagneux, P.; Pribat, D. Field electron emission from individual carbon nanotubes of a vertically aligned array. Appl. Phys. Lett. 2002, 81, 343-345.

69. Yamaguchi, H.; Murakami, K.; Eda, G.; Fujita, T.; Guan, P.; Wang, W.; Gong, C.; Boisse, J.; Miller, S.; Acik, M. Field emission from atomically thin edges of reduced graphene oxide. Acs Nano 2011, 5, 4945-4952.

70. Wang, Y.; Yang, Y.; Zhao, Z.; Zhang, C.; Wu, Y. Local electron field emission study of two-dimensional carbon. Appl. Phys. Lett. 2013, 103, 033115.

71. Shao, X.; Srinivasan, A.; Ang, W.K.; Khursheed, A. A high-brightness large-diameter graphene coated point cathode field emission electron source. Nat. Commun. 2018, 9, 1288.

72. Swanson, L.; Martin, N. Field electron cathode stability studies: Zirconium/tungsten thermal-field cathode. J. Appl. Phys. 1975, 46, 2029-2050.

73. Khursheed, A. Design of a focused electron beam column for ring-cathode sources. Ultramicroscopy 2013, 128, 10-23.

74. Khursheed, A.; Ang, W.K. Annular focused electron/ion beams for combining high spatial resolution with high probe current. Microsc. Microanal. 2016, 22, 948-954.

75. Nguyen, D.D.; Suzuki, S.; Kato, S.; To, B.D.; Hsu, C.C.; Murata, H.; Rokuta, E.; Tai, N.-H.; Yoshimura, M. Macroscopic, freestanding, and tubular graphene architectures fabricated via thermal annealing. ACS nano 2015, 9, 3206-3214.

76. Shao, X.; Srinivasan, A.; Zhao, Y.; Khursheed, A. A few-layer graphene ring-cathode field emitter for focused electron/ion beam applications. Carbon 2016, 110, 378-383.